J. Physiol. (1980), **304** *pp.* 231–249
With 10 *text-figures*
Printed in Great Britain

VOLTAGE CLAMP OF CAT MOTONEURONE SOMATA: PROPERTIES OF THE FAST INWARD CURRENT

BY JOHN N. BARRETT AND WAYNE E. CRILL

From the Department of Physiology and Biophysics, University of Miami School of Medicine, P.O. Box 016430, Miami, Florida, 33101, the Division of Neurology, Veterans Administration Hospital, Seattle, Washington, 98108, and the Department of Physiology and Biophysics, University of Washington School of Medicine, Seattle, Washington, 98195, U.S.A.*

(*Received 14 September 1978*)

SUMMARY

1. The soma membrane of cat spinal motoneurones was voltage clamped using separate intracellular voltage and current electrodes directed into the same motoneurone with a new guide system.

2. Antidromic stimulation of the motoneurone's axon or small depolarizing voltage clamp steps (10–20 mV from the resting potential) evoked a small (30–80 nA) all-or-none action potential current, which was shown by occlusion experiments to originate from the initial segment of the axon. Except for this axonal current spike, there was no indication of active (voltage-dependent) conductance changes in membrane regions not under good voltage clamp control. Calculations based on motoneuronal geometry, and electrophysiological recordings from spinal cord neurones in tissue culture, indicate that the proximal portions of dendritic membranes were also under good voltage clamp control.

3. Clamp depolarizations greater than 20 mV activated a fast, transient inward current, which increased in a smoothly graded manner with depolarization between 20 and 40 mV from the resting potential, reaching a peak magnitude of up to 450 nA, and then decreased smoothly for larger depolarizations. Extrapolation of the current–voltage relationship for this current indicated a reversal potential about 80–116 mV positive to the resting potential.

4. This transient inward current is blocked by tetrodotoxin. After a depolarizing voltage clamp step the conductance system controlling this current first activates with fast, non-linear kinetics, and then inactivates with first-order kinetics. These properties are similar to those of the Na conductance system in squid and frog axons.

5. Conditioning-testing experiments showed that the time constant of inactivation ranges from 1·0–1·3 msec at potentials slightly negative to the resting potential to 0·1–0·3 msec for depolarizations 60 mV from the resting potential. The degree of steady-state inactivation also varied with membrane potential, ranging from total inactivation at depolarizations greater than 30 mV from the resting potential, to minimal inactivation at potentials more than 10 mV negative to the resting potential.

* Please address all correspondence and reprint requests to J. N. Barrett at this address.

0022-3751/80/8780-0733 $07.50

INTRODUCTION

Experiments using voltage-clamp techniques have demonstrated that the action potentials in many excitable tissues are produced by a sequence of voltage-dependent changes in membrane ionic conductances (Hodgkin & Huxley, 1952*b*; reviewed in Hille, 1970). Extending these voltage clamp techniques to small, geometrically complex and poorly accessible cells such as vertebrate central neurones has proved difficult. Previous voltage clamp studies of cat motoneurones by Araki & Terzuolo (1962) and Nelson & Frank (1964) have demonstrated fast inward and slower outward conductance changes associated with the depolarizing and repolarizing phases of the motoneurone action potential. The present study describes an improved voltage clamp system for cat motoneurones, and presents evidence that the major portion of the voltage clamp currents recorded in selected motoneurones arise from conductance changes originating on, or electrically close to, the voltage-clamped soma. The kinetics of the fast inward current are also described. The following paper (Barrett, Barrett & Crill, 1980) describes three outward current systems in cat motoneurones, and uses the measured passive and active properties of the motoneurone membrane to reconstruct the action potential evoked in an unclamped motoneurone.

METHODS

Spinal cord preparation

Adult cats (1·5–2·5 kg) were anaesthetized with Nembutal (Abbott), an initial I.P. dose of 35 mg/kg, followed by I.V. supplements of about 0·5 mg/kg.hr. A bilateral pneumothorax was performed, and animals were artificially respirated. Flaxedil was given in the minimal dose required to produce muscle paralysis. The lumbar enlargement of the spinal cord was exposed using standard laminectomy procedures. The dura was removed from the dorsal surface of the cord, and the exposed cord was covered with mineral oil to prevent desiccation. The animal's rectal temperature was maintained at 37 ± 1 °C by a temperature control system consisting of a ventral heating pad and a hair dryer which blew warm air into a plastic bag surrounding the animal. The temperature of the mineral oil bath covering the spinal cord was maintained at 37 ± 1 °C by a small heat lamp.

Micro-electrode construction and placement

Lumbar motoneurones were impaled with two intracellular micro-electrodes, one to inject current into the cell, the other to record transmembrane voltage. These micro-electrodes were drawn from glass tubing 1 mm in diameter, and their tips were bevelled on a rotating ruby rod (Barrett & Whitlock, 1973; for other bevelling techniques see Kripke & Ogden, 1974; Brown & Flaming, 1975; Odgen, Citron & Pierantoni, 1978). The largest diameter of the electrode tip opening was about 1 μm. These micropipettes were filled with a relatively dilute (0·2–0·5 M) aqueous solution of KCl. The micro-electrodes had resistances of 5–20 MΩ, and could deliver relatively large transient currents into the motoneurones without blocking or filling the neurones with excessive amounts of KCl. The current electrode was shielded as detailed below.

The current and voltage micro-electrodes were directed into the same motoneurone using the guide system illustrated in Fig. 1. A tapering guide pipette was constructed from 3–4 mm diameter glass tubing with a theta-shaped cross-sectional area, drawn to a tip diameter of about 10 μm. The current and voltage micro-electrodes, held by a miniature mechanical micromanipulator for two electrodes (Narashigi), were inserted under microscopic control down separate barrels of the theta-tubing guide pipette, and positioned such that their tips were within 5–15 μm of each other. The dual mechanical micromanipulator was mounted on the moving shaft of a hydraulic micromanipulator, which allowed coupled movement of the current and voltage

micro-electrodes within the guide pipette. The hydraulic manipulator setting at which the two micro-electrode tips just emerged from the tip of the guide pipette was noted using a microscope (100–400 ×) to view the electrode tips.

The entire array of current and voltage micro-electrodes plus guide pipette was advanced together through the spinal cord by a base micromanipulator (Kopf). As the electrode array moved through the pia and white matter, the tips of the current and voltage micro-electrodes were withdrawn into the guide pipette to prevent breakage. The antidromic field potential evoked by stimulating muscle nerves was used to indicate proximity to the motoneurone pool. When this potential grew large, the current and voltage micro-electrodes were advanced together using the hydraulic manipulator until the manipulator setting indicated that the tips of these electrodes protruded 10–30 μm from the tip of the guide pipette. The entire electrode array was

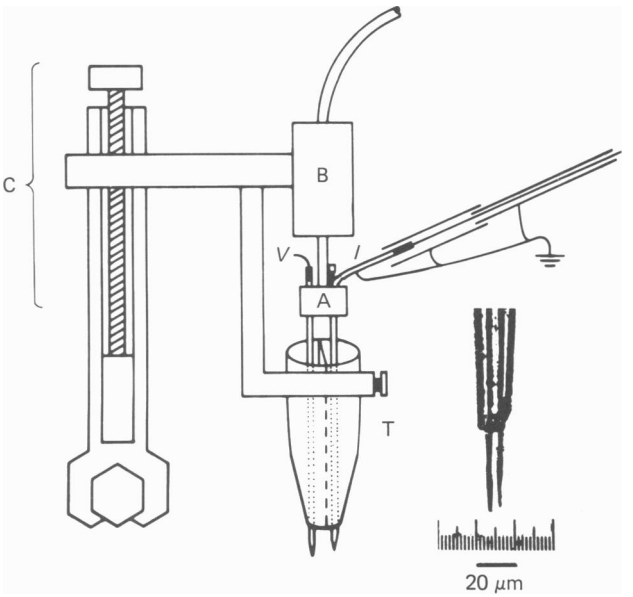

Fig. 1. Diagram of apparatus used to insert two separate micro-electrodes into the same motoneurone soma. The current-injecting (I) and voltage-recording (V) electrodes are aligned under microscopic control using a small mechanical micromanipulator (A). This manipulator is attached to the moving shaft of a hydraulic micromanipulator (B), which is used to guide the electrodes down separate barrels of a tapered pipette drawn from theta tubing. The entire system is driven through the spinal cord using a large mechanical manipulator (C). The inset photograph shows the tips of the current and voltage electrodes protruding from the theta-tubing guide pipette. Further details in text.

then driven forward using the base manipulator until both current and voltage electrodes impaled the same motoneurone soma. Impalements were judged successful if the measured resting potential was at least as negative as −55 mV, if both current and voltage electrodes recorded identical 60–80 mV antidromic action potentials, and if current passed through either electrode was equally effective in evoking an action potential. After a successful impalement, the current electrode was disconnected from its voltage-recording pre-amplifier and connected to the current delivery system of the voltage clamp circuit.

Accurate voltage clamp measurement of transient currents requires a system with very low resistive and capacitative coupling between the current and voltage electrodes. In our system the resistive coupling between the separate current and voltage electrodes was only 0·001–0·01 MΩ, compared to a motoneurone input resistance of 0·5–2 MΩ. To reduce capacitative coupling between the current and voltage electrodes the current electrode was shielded to within a few

mm of its tip with a layer of electrically conducting silver paint (Walsco 21-2). An additional shield surrounded the top of the shaft of the current electrode and the wire which delivered current from the output of the voltage clamp circuit (Fig. 1). Both current electrode shields were grounded through a switch which allowed them to be ungrounded when the voltage clamp was

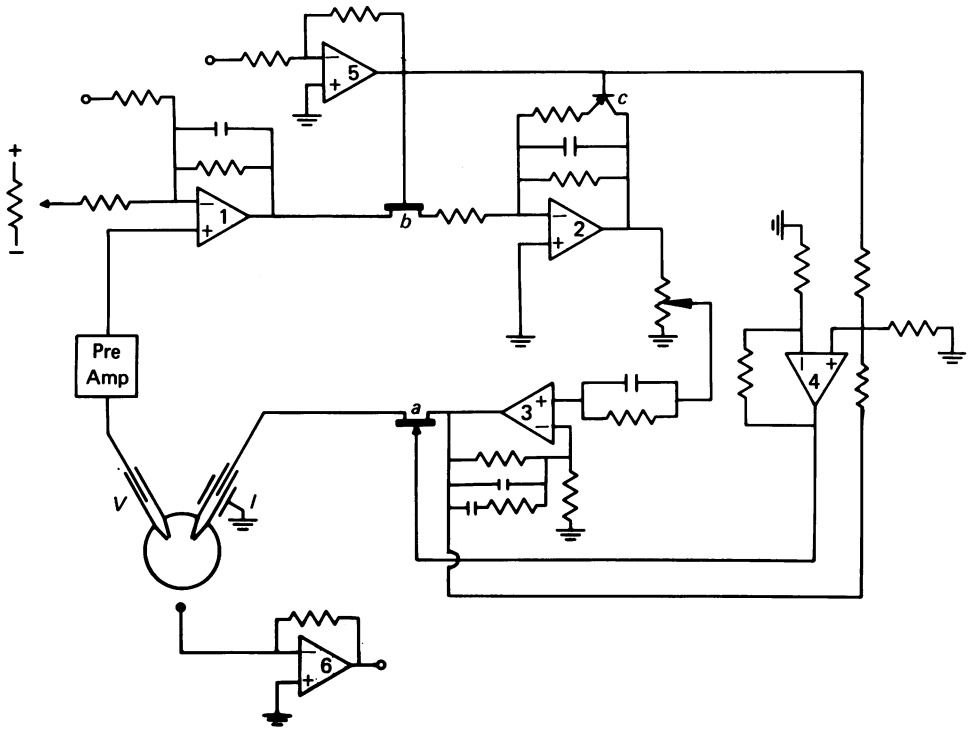

Fig. 2. Circuit used to voltage-clamp motoneurone somata. The signal from the voltage-recording electrode (*V*) was led via a short (7 cm) silver wire into a unity-gain, high input impedance pre-amplifier (Picometric 181), and was then compared with the command signal by operational amplifier 1. The error signal was amplified and inverted by amplifiers 2 and 3. High-voltage (± 100 V) amplifier 3 controls the frequency response of the circuit; its output voltage was applied directly to the shielded current-injecting electrode (*I*) when the circuit was in the clamp mode. The circuit was switched between clamp and non-clamp modes by an electronic switching system in which a high-voltage operational amplifier (no. 4) controls the gate voltage on a field-effect transistor (*a*) between the current-injecting electrode and amplifier 3, and transistors *b* and *c* control the gain of amplifier 2. The switching signal voltage is applied to the base of these three transistors through operational amplifier 5. The voltage clamp current was monitored by a virtual ground amplifier (no. 6) system attached to a silver chloride-coated silver wire placed under the skin of the animal. With larger animals it was necessary to shield the preparation with a grounded conducting screen cage to avoid excess 60 Hz noise in the virtual ground circuit. The outputs of the pre-amplifier and virtual ground circuit were amplified and monitored by a Tektronix 565 oscilloscope (not shown).

not in use. This shielding system was so effective that a 5 V pulse applied directly to the current electrode produced a capacitative transient of less than 0·5 mV in the voltage electrode. The tips of both barrels of the theta guide pipette were filled with mineral oil to insulate the grounded current electrode shields from the virtual ground circuit used to record voltage clamp current.

Voltage clamp circuit

The voltage clamp circuit (Fig. 2) employed a transistor switch system similar in principle to that of Bezanilla, Rojas & Taylor (1970), which allowed rapid (< 50 μsec) and artifact-free switching between the voltage-recording mode (constant current stimulation) and the voltage clamp mode. During most experiments the voltage clamp mode was used only while taking measurements during the first 50–500 msec of each 1 sec intertrial interval. This procedure allowed us to monitor the stability of the resting and action potentials during the course of the experiment.

The voltage clamp circuit had a steady-state gain of 50000–100000 between the unity-gain pre-amplifier and the current electrode. This high voltage gain was required to drive sufficient clamp current through the resistance of the current electrode (5–20 MΩ). When this electrode resistance is included to give the complete loop gain of the circuit, the total gain from the voltage electrode to the current injected through the current electrode was about 10^{-5} A/mV error signal at 0 Hz, falling to about 10^{-9} A/mV at 10 kHz. The circuit could clamp the soma voltage to any desired level within 50 mV of the resting potential in about 0·2 msec.

All clamp potentials are expressed relative to the resting potential. Thus, for example, clamp potentials of $+50$ and -12 mV refer, respectively, to potentials 50 mV positive and 12 mV negative to the resting potential. By convention, inward clamp currents are pictured as downward deflexions. Most of the illustrated records in this and the following paper came from a single motoneurone, but all reported phenomena were observed in at least ten motoneurones.

RESULTS

Passive capacitative currents: charging transients

Small depolarizing voltage clamp steps (less than 5 mV) produce a transient outward capacitative current, followed by a steady outward current. The steady outward current reflects the steady-state passive input resistance of the motoneurone, which ranged from 0·6 to 2 MΩ in the motoneurones studied here. The capacitative current was not instantaneous due to the distributed nature of the dendritic membrane capacitance. When the decaying phase of the capacitative current transient was analysed as a sum of exponential components, the components of largest amplitude had time constants of 0·5 msec or less. The longest charging time constant was 2·5–3 msec, about half the longest passive membrane time constant of the motoneurones (5–7 msec). This ratio between the longest charging time constant and the longest passive membrane time constant is roughly consistent with Rall's (1969) calculations for a neurone model which approximates the dendritic membranes as an equivalent cylinder of electrotonic length $1{\cdot}5\lambda$, near the average electrotonic length estimated for motoneurone dendrites (Lux, Schubert & Kreutzberg, 1970; Nelson & Lux, 1970; Burke & ten Bruggencate, 1971; Jack & Redman, 1971; Barrett & Crill, 1974*a*).

Where necessary, we subtracted the capacitative current, $I_c(t)$, from the clamp current records by assuming that the magnitude of the capacitative current was proportional to the magnitude of the voltage step, ΔV, and had a time course similar to that of the voltage clamp currents measured following small, subthreshold voltage clamp steps. Eqn. (1), used for most corrections, corrects for only the slowest time constant of this subthreshold current response:

$$I_c(t) = (0{\cdot}5\ \mu\text{mho})\ \Delta V\ (\exp(-t/0{\cdot}5\ \tau_0)), \tag{1}$$

where τ_0 is the longest passive time constant of the motoneurone membrane, 5 msec

for the motoneurone shown in most subsequent Figures. The conductance factor in this equation is scaled according to the input resistance of the motoneurone; the value 0·5 μmho applies to a motoneurone with an input resistance of 1 MΩ. This equation for calculating capacitative currents assumes that the non-clamped remote dendrites have no major voltage-sensitive conductance changes (see below).

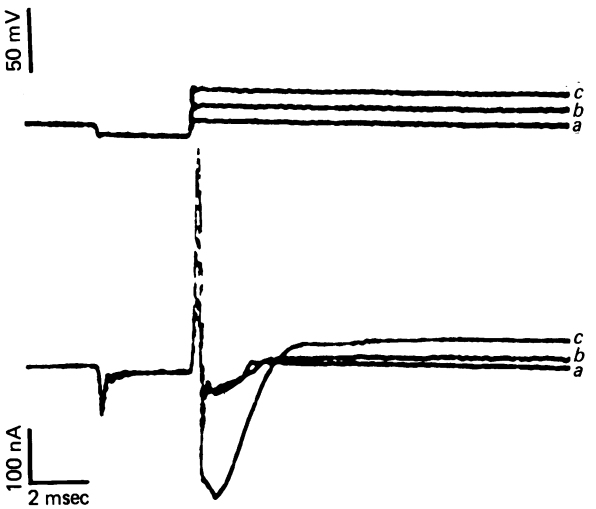

Fig. 3. Activation of initial-segment action current and fast inward current by small voltage-clamp depolarizations. The motoneurone was hyperpolarized to −9 mV for 3 msec and then depolarized to varying levels, labelled *a*, *b*, *c* in the upper trace. The corresponding clamp currents (labelled *a*, *b*, *c*) are superimposed in the lower trace. The surge of outward current accompanying the step depolarization charges the capacitance of the soma and dendritic membranes. In traces *a* and *b* this capacitative current is followed by a small (60 nA), all-or-nothing inward current due to an action potential in the non-clamped initial segment of the axon. The larger depolarization of trace *c* activates in addition a portion of the fast inward current system in the soma membrane.

Initial segment action currents

Voltage clamp step depolarizations in the range of 5–20 mV positive to the resting potential produced a brief, all-or-nothing inward current, as illustrated in traces *a* and *b* of Fig. 3. The illustrated current has a peak amplitude of 60 nA; peak amplitudes ranged from 30 to 80 nA in our motoneurone sample. This current developed suddenly, and in a given motoneurone its amplitude remained constant over this voltage range (5–20 mV), indicating that it originated from a region that was not under voltage-clamp control. A similar all-or-nothing inward current could be evoked by stimulating the ventral roots while clamping the soma membrane to the resting potential. The inward currents produced by the 5–20 mV depolarizing clamp steps and by antidromic stimulation occluded each other, leading us to conclude, in agreement with Araki & Terzuolo (1962), that this brief inward current arises from an action potential in the initial segment of the axon.

For this study we selected motoneurones which showed only one initial-segment current spike at the onset of a depolarizing voltage clamp step. Other motoneurones

with equally acceptable resting potentials, action potentials and voltage clamp currents gave repetitive initial segment action currents during a depolarizing voltage clamp step. One explanation for this different discharge pattern might be that repetitively discharging initial segments were longer, thinner and thus electrically more remote from the voltage-clamped soma than initial segments that gave only a single discharge before inactivating. This suggestion is supported by our observation

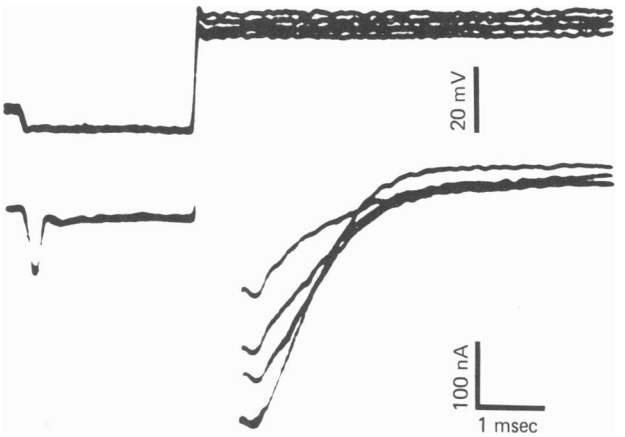

Fig. 4. Graded activation of fast inward current (lower records) by voltage-clamp step depolarizations. The motoneurone was hyperpolarized to −6 mV for 2·5 msec and then depolarized to various levels ranging from 21 to 28 mV positive to the resting potential (upper records). A large capacitative current during the first 0·6 msec following the depolarizing step obscures the ionic currents present during that time.

that the repetitive action currents tended to be smaller than the single action currents, and by Conradi's (1969) report that some motoneurone initial segment regions are short (100 μm) and broad, while others are long (300 μm) and thin.

The fast inward current began to appear at depolarizations exceeding about 20 mV (trace *c* of Fig. 3; Fig. 4). The various methods used to correct these inward current records for the superimposed initial segment action current are described where appropriate.

Tests for voltage-sensitive inward currents in remote dendrites

Fig. 4 shows the fast, transient (2–3 msec) inward currents evoked in one motoneurone by step depolarizations of 21–28 mV. Over this voltage range the amplitude of this inward current increased in a smoothly graded manner with increasing depolarization. This inward current was followed by an outward current whose magnitude also increased with increasing depolarization (Fig. 4). The uppermost curve in Fig. 5 plots the magnitude of the steady-state outward current as a function of clamp voltage. Outward currents evoked by depolarization are analysed more completely in the following paper (Barrett *et al.* 1980).

Before analysing the voltage-sensitive inward and outward conductance systems in the voltage-clamped soma, it was necessary to estimate the extent to which the recorded currents were contaminated by currents from electrically distant regions

of the dendritic membrane. Calculations using measured motoneuronal geometries indicate that most of the proximal dendritic membranes are so electrically close to the soma that they would be under good voltage clamp control (Barrett & Crill, 1974*b*). For example, at a frequency of 100 Hz the space constant of a dendrite 5 μm

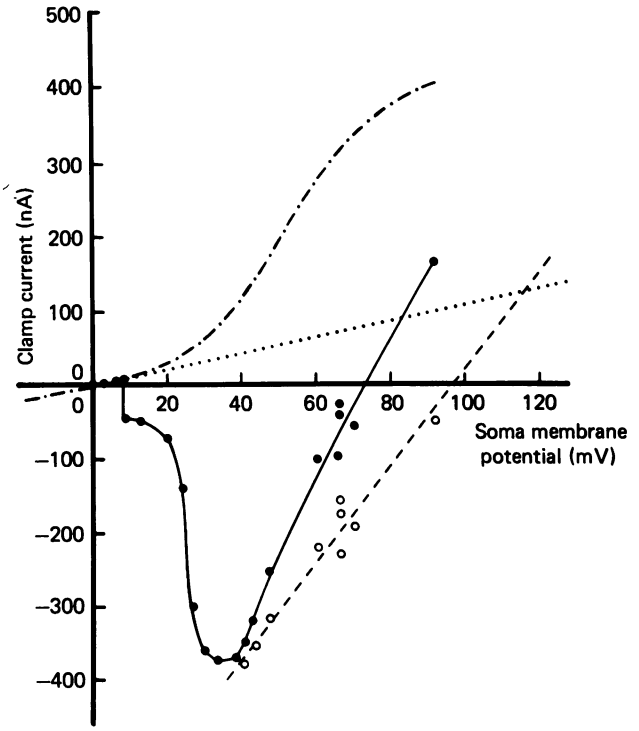

Fig. 5. Current–voltage relationships measured in the steady-state (dash–dot line) and at the time of the peak inward current (filled circles, continuous line). The inward current plateau in the region of 10–20 mV is due to the all-or-nothing action current from the unclamped initial segment of the axon. The dotted line, extrapolated from the steady-state current–voltage relationship measured near the resting potential, gives the expected passive leakage current. The line drawn through the measured peak inward currents (filled circles) intersects the leakage current line at +83 mV, a lower bound estimate of the inward current reversal potential. Open circles plot peak inward currents corrected for superimposed capacitative and outward currents; the dashed line drawn through these corrected current values yields a revised estimate of +116 mV for the inward current reversal potential. All voltages are measured relative to the resting potential.

in diameter is 350 μm, assuming a normal resting specific membrane resistance of 2000 Ωcm^2. These calculations are supported by direct electrical recordings in tissue-cultured rat and mouse motoneurones: intracellular recordings of action potentials in proximal dendrites are identical to action potentials recorded simultaneously in the soma, even when relatively large depolarizing or hyperpolarizing currents are applied to the soma (Peacock, Nelson & Gladstone, 1973, and observations of J. Barrett). Only dendritic membrane regions more than about 200 μm from the soma are electrically distant enough to introduce artifacts into the clamp current

records. If these remote dendrites behave as passive cable structures, then the currents they draw can be estimated and subtracted (eqn. (1)). However, any large, voltage-sensitive conductance changes in non-clamped dendritic membranes would complicate interpretation of recorded somatic clamp currents. Isolated dendritic action potentials have not been recorded in normal cat motoneurones, but they have been found in cat motoneurones undergoing chromatolysis (Eccles, Libet & Young, 1958; Kuno & Llinás, 1970).

Our voltage clamp records (e.g. Figs. 4, 5) revealed no evidence of substantial active currents in remote dendrites. Except for the small, all-or-nothing current spike from the initial segment of the axon, both inward and outward currents changed in a continuous manner with increasing depolarization; no additional all-or-nothing components were detected. To test further for conductance changes in remote dendrites, we superimposed a small voltage clamp step on top of different holding voltages and found that the capacitative charging transient decreased by less than 10% as holding voltages increased from the resting potential to +50 mV. This result indicates that the amount of current necessary to charge remote dendritic membranes remains fairly constant over this voltage range, arguing against large conductance changes in non-clamped dendritic membranes.

In another test to uncover active currents from remote dendrites, we first clamped the soma to +15 mV to elicit and subsequently inactivate the initial segment action current, and then stepped the voltage to more depolarized levels. This second depolarizing step evoked no detectable all-or-nothing current response, but rather a graded activation of inward and outward currents. We also attempted to elicit active responses from remote dendrites by superimposing an excitatory postsynaptic potential (evoked by dorsal root or peripheral nerve stimulation) on top of various depolarizing clamp steps and ramps. Never did the synaptic potential activate any all-or-nothing current component.

These results indicate that under our experimental conditions distal dendrites do not generate detectable all-or-nothing action potentials or large voltage-dependent conductance changes when the motoneurone soma is voltage-clamped. Thus the inward and outward currents illustrated in Fig. 4 are not seriously contaminated by uncontrolled active dendritic currents. These experiments do not of course prove that remote dendrites are devoid of any voltage-dependent conductances.

Voltage-sensitive fast inward current

Reversal potential and tetrodotoxin sensitivity

The filled circles in Fig. 5 plot the peak amplitude of the transient inward current as a function of the clamped soma voltage. The latency of the peak inward current gradually shifted from 0·9 msec for 20 mV step depolarizations to 0·5 msec for 80 mV step depolarizations. The peak inward current increased with increasing depolarization over the range 20–35 mV, reaching a peak amplitude of 380 nA in this motoneurone. Peak inward current amplitudes ranged from 175 to 450 nA in our motoneurone sample; the larger peak currents are probably associated with larger motoneurones. The peak inward current decreased with increasing depolarization above 40 mV. Assuming that this decrease in inward current magnitude was due

primarily to reduction of the inward current driving potential, we estimated the reversal potential of the inward current as the (extrapolated) intersection of the curve plotting peak amplitude (filled circles, Fig. 5) with the diagonal dotted line extrapolated from passive leakage current measurements in the region of the resting potential. This intersection occurred at about +83 mV (relative to the resting potential). It underestimates the true reversal potential because of capacitative and active outward potassium currents also present at this time. The dashed line in Fig. 5 corrects for the capacitative current using eqn. (1) and for the superimposed outward current using data from the following paper (Barrett *et al.* 1980). The corrected inward current reversal potential is approximately +116 mV. Estimated inward current reversal potentials ranged from 80 to 116 mV in our motoneurone sample. Using a similar technique, Araki & Terzuolo (1962) estimated a reversal potential of +120 mV for the transient inward current.

The inward current amplitudes plotted in Fig. 5 were not corrected for the initial segment action current. If this initial segment current has a voltage dependence similar to that of the fast inward current (i.e. if it decreases with increasing depolarization above 40 mV, and has the same reversal potential), then this extraneous current will not affect our estimates of the inward current reversal potential. If instead the initial segment current changes relatively little with increasing depolarization, then our estimated reversal potentials are too high; for example, subtracting a constant 60 nA initial segment current from the inward current amplitudes of Fig. 5 yields an estimated reversal potential of 108 mV rather than 116 mV.

Attempts to reverse the fast inward current using very large step depolarizations gave unconvincing results, mainly because the capacitative charging transient became enormous, obscuring the fast inward current.

The fast inward current was blocked by application of 10^{-4} M-tetrodotoxin to the electrode entry zone of the spinal cord, consistent with Blankenship's (1968) report that tetrodotoxin blocks motoneurone action potentials in the cat.

Voltage-dependent inactivation

Fast sodium currents in most excitable tissues are first activated and then inactivated by depolarization, and the transient nature of the inward currents illustrated in Fig. 4 suggests that the fast inward current in cat motoneurones shows similar activation–inactivation behaviour during prolonged depolarizations. To test more rigorously for depolarization-sensitive inactivation, we used Hodgkin & Huxley's (1952*a*) technique of applying a conditioning depolarization followed after a variable interval by a test depolarization. The superimposed current records of Fig. 6 demonstrate this inactivation: as the interval between the conditioning and testing pulses is shortened, the peak inward current evoked by the test voltage step is progressively reduced.

To measure this inactivation more accurately, we corrected the recorded inward currents by subtracting the capacitative current (eqn. (1)) and the predicted outward currents (Barrett *et al.* 1980). For conditioning and testing pulses smaller than 35 mV these corrections were less than 10% of the control peak inward current. Peak inward currents were also corrected for the superimposed initial segment action current, by assuming that the initial segment current evoked by the test depolariza-

tion was the same as that observed during smaller test depolarizations at the same conditioning–testing interval. This correction was reasonably accurate because the test depolarizations that evoked maximal inward currents (+36 mV in Fig. 6) were not much larger than the 10–15 mV depolarizations used to estimate the initial segment current.

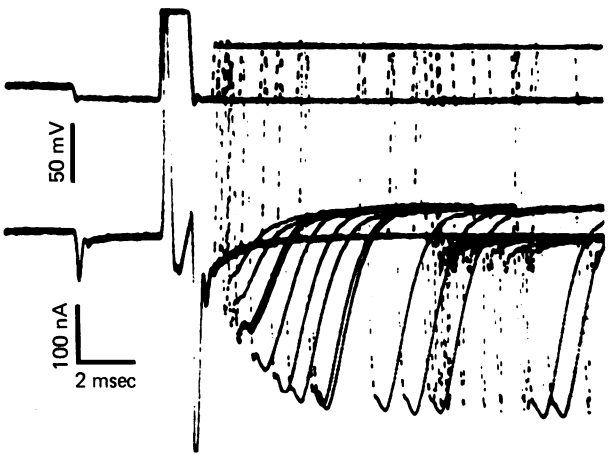

Fig. 6. Effect of conditioning depolarization on the fast inward current. As indicated by the superimposed voltage records in the upper trace, the membrane was hyperpolarized to −11 mV for 3 msec, depolarized to +66 mV for 1 msec (conditioning depolarization), repolarized to −11 mV and then after a variable delay depolarized to +36 mV for 7 msec (test depolarization). The superimposed current records in the lower trace indicate that the test inward current becomes progressively smaller as the interval between the conditioning and test depolarizations is decreased, an effect due to both the inactivation of the fast inward conductance system and the activation of outward currents produced by the conditioning depolarization.

Experiments similar to that of Fig. 6 were repeated, varying the magnitude and duration of the conditioning depolarization or the holding potential during the conditioning–test interval, in order to determine how the rates of development and decay of inactivation and the steady-state level of inactivation vary with membrane voltage. Fig. 7 is a semilogarithmic plot of the decay of inactivation of the fast inward current as a function of time following a conditioning depolarization. Inactivation is defined conventionally as $(1-h(t))$, where

$$h(t) = I_{Na}(t)/I_{Na}(\infty).$$

In this formulation, h represents that fraction of the fast inward conductance system that is available for activation, $I_{Na}(t)$ is the (corrected) peak inward current evoked by a test depolarization administered at time t following the end of the conditioning pulse, and $I_{Na}(\infty)$ is the peak inward current evoked by the test depolarization in the absence of any conditioning depolarization. Plotted data were obtained from the same motoneurone as in Fig. 6, using a similar clamp paradigm, except that the conditioning depolarization was smaller, to reduce outward current activation, and longer, to increase inward current inactivation. The data points are well fitted by a straight line, suggesting that recovery from inactivation can be described as a simple

exponential process with a time constant of 1 msec at −11 mV, the membrane potential during the interval between the conditioning and test depolarizations. Analysis of similar experiments done at different inter-stimulus holding potentials indicated that the time constant of decay of inactivation decreased as the holding potential became more depolarized (see Fig. 8).

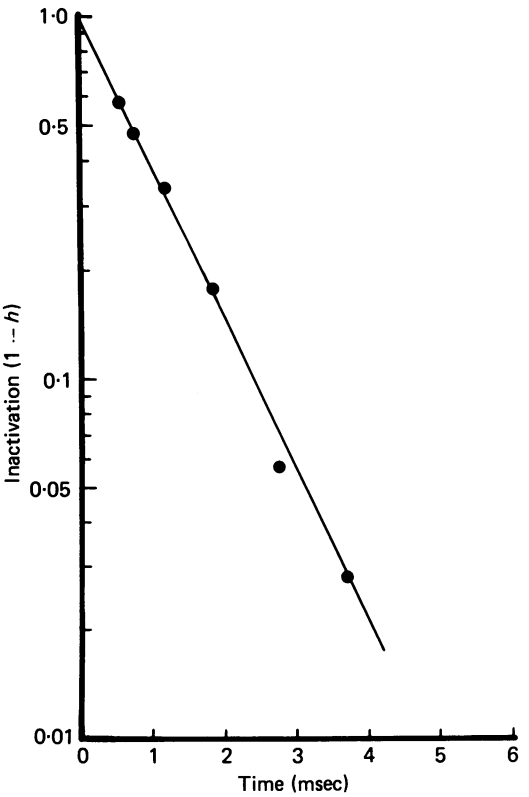

Fig. 7. Semilogarithmic plot of the time course of recovery from inactivation of the fast inward conductance system at −11 mV. Data were obtained using a conditioning-test paradigm like that of Fig. 6 except that the conditioning depolarization was smaller and longer (30 mV, 10 msec). Inactivation $(1-h)$ was calculated using test inward currents corrected for superimposed outward, capacitative and initial segment currents, as described in the text. The inactivation values are well fitted by a straight line, suggesting an exponential decay. There was a delay between the onset of the test depolarization and measurement of the peak inward current. As long as h_∞ at the test voltage is small (test depolarization $\geqslant$ 30 mV), the ratio of the test h value to the control h value is independent of this delay provided that test and control Na current measurements are made with the same delay following the onset of the clamp depolarization (see Hodgkin & Huxley, 1952*a*).

Extrapolation of the inactivation line of Fig. 7 back to a conditioning–test interval of zero yields an estimate of the total inward current inactivation, 1-h, produced by the conditioning depolarization, near 100% in this case. When this analysis was repeated for shorter conditioning depolarizations, it was found that semilogarithmic plots of h *vs.* the duration of the conditioning depolarization were linear, indicating

that the development of inactivation can also be characterized as a single exponential process. The time constant of development of inactivation decreased as the magnitude of the conditioning depolarization increased. If the inactivation process in cat motoneurones is similar to that in squid axons, the time constant for recovery from inactivation at a particular holding potential should equal the time constant for the development of inactivation at that potential. This equality was satisfied within

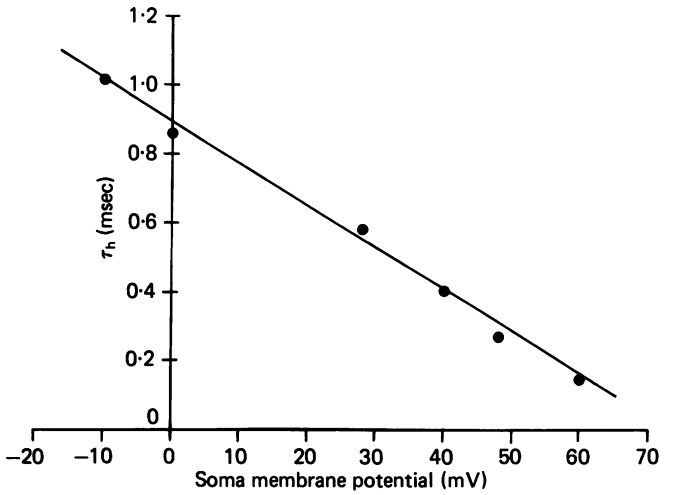

Fig. 8. Voltage dependence of the time constant of inactivation of the fast inward current, τ_h. For voltages near the resting potential, τ_h was calculated from the decay of inactivation following a conditioning depolarization, as shown in Fig. 7. For large depolarizations from the resting potential, τ_h was calculated from the rate of development of inactivation during a conditioning depolarization, as described in the text.

experimental error over the narrow range of membrane voltages (+10 to +20 mV) in which both time constants were measured. Thus the time constants of development and decay of inactivation measured in a single motoneurone were combined, as in Fig. 8, to show how the time constant of inactivation, τ_h, varies with membrane voltage over the range −10 to +60 mV.

The other motoneurones in our sample showed a similar voltage dependence for τ_h. Minimal τ_h values of 0·1–0·3 msec occurred at depolarizations near 50 mV, while maximal τ_h values of 1·0–1·3 msec occurred at membrane potentials 10–15 mV below the resting potential.

The degree of inward current inactivation following a long (10 msec) conditioning depolarization gives a measure of the steady-state inactivation, $1-h_\infty$, of the inward current at that membrane potential. Fig. 9 shows how the parameter h_∞ varied with membrane potential in one motoneurone. Other motoneurones showed a similar voltage dependence for h_∞, with the peak value of 1·0 at potentials about 10 mV negative to the resting potential, dropping to values near zero for depolarizations greater than 25–30 mV from the resting potential. Thus the steady-state inactivation of the fast inward current, $1-h_\infty$, increases with increasing depolarization, and is essentially complete at depolarizations exceeding +30 mV from the resting potential. This result is similar to the nearly complete steady-state inactivation of the fast

inward current at depolarized potentials in frog node (Conti, Hille, Neumcke, Nonner & Stampfli, 1976).

The data presented in Figs. 6–9 suggest that the depolarization-induced inactivation of the fast inward current in cat motoneurones is similar to that described for squid axons by Hodgkin & Huxley (1952*a*, *b*). In both preparations, a sudden change

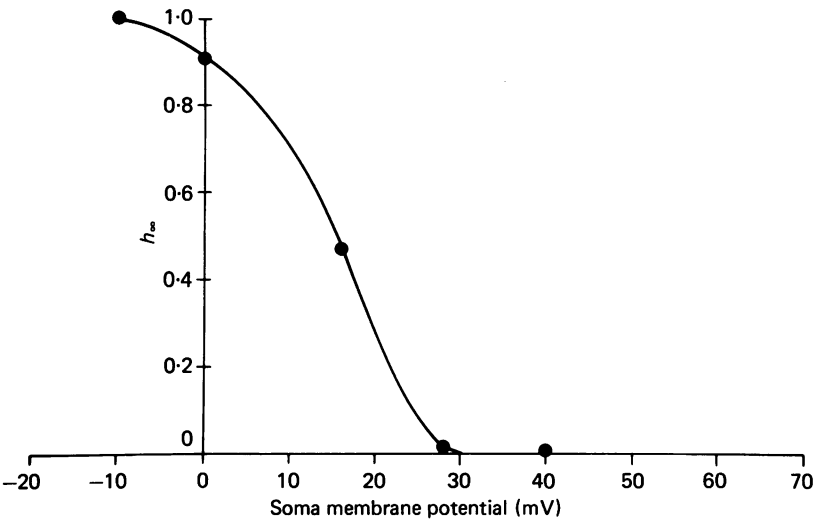

Fig. 9. Voltage dependence of the steady-state inactivation parameter, h_∞, in the motoneurone of Fig. 8. h_∞ was calculated from the extrapolated 'zero-time' value of inactivation, $1-h(t)$, following long conditioning depolarizations of the indicated magnitude.

in clamp potential causes the inactivation parameter, $1-h\,(V, t)$, to approach its new steady-state value, $1-h_\infty\,(V)$, along an exponential time course (time constant $= \tau_h$), where both h_∞ and τ_h are functions only of the new clamp potential. Thus at any given membrane potential, the change in h with time can be described by the equation:

$$\frac{dh(t)}{dt} = \frac{1}{\tau_h}\,(h_\infty - h(t)).$$

Recent work in squid and *Myxicola* axons and frog nodes indicates that the onset of inactivation following a depolarizing clamp step is delayed rather than perfectly exponential (Hille, 1976; Bezanilla & Armstrong, 1977; Chiu, 1977). This finding would suggest that inactivation is not a simple first-order process, and/or that inactivation requires prior activation of fast inward current channels. The time resolution in our experiments was not adequate to determine whether inactivation might be similarly delayed in cat motoneurones.

Voltage-dependent activation

The time course of activation of the inward current produced by depolarizing clamp steps was difficult to measure because of contamination by capacitative,

initial segment and depolarization-activated outward currents. A stimulation pattern that overcame some of these difficulties consisted of applying short step depolarizations (0·1–3 msec), followed immediately by a hyperpolarizing voltage step to the reversal potential for the outward currents (-6 to -20 mV). At this final potential inward current tails should not be contaminated by 'active' outward currents. Current tails recorded after prolonged depolarizing steps were assumed to be entirely capacitative, and this estimated capacitative current was subtracted from the inward current tails measured following shorter depolarizations (this procedure overcorrects for capacitative currents following pulses too short to charge the dendritic capacitance completely, but for pulse lengths of 0·3–1·5 msec the capacitative correction was less than 10% of the total current). After very short depolarizing steps, inward current tails were also contaminated by the small active current from the initial segment. We attempted to correct for this initial segment current by subtracting from the inward current tails the initial segment current recorded following brief, small depolarizations. However, since the magnitude and time course of the initial segment action potential probably change during intense depolarization of the soma, this method of correcting for initial segment currents may be subject to considerable error. Thus, because of the uncertainties involved in correcting for superimposed capacitative and initial segment currents, our characterization of the activation kinetics of the fast inward current must be considered tentative.

After the capacitative and initial segment artifacts were subtracted, the remaining inward current tail decayed exponentially with a time constant of about 1 msec at -13 mV. Extrapolation of this current tail to the end of the depolarizing voltage step gave an estimate of the amount of inward current activated at the end of that depolarization. The filled circles in Fig. 10 plot these extrapolated current values as a function of the duration of a 30 mV depolarizing step. The inward current first increases with increasing duration of the depolarizing step, reaching a peak value for depolarizations lasting 0·5–1 msec, and then decreases for longer depolarizations as inactivation increases. Since with this voltage-clamping pattern active outward currents did not contaminate the inward current tails, the decrease in peak inward current observed following depolarizations exceeding 1 msec demonstrates that inactivation of the inward current is not merely an artifact due to depolarization-induced activation of opposing outward currents.

Data similar to that of Fig. 10 were collected for a range of depolarizations, but large capacitative currents reduced the accuracy of the inward current measurements following large depolarizations ($>$ 80 mV). The inward current appeared to activate faster at higher depolarizations.

In the Hodgkin–Huxley model of the inward current in squid axons, the total conductance of the inward current channels is proportional to the product of an activation term M and a potential activation term h (where $1-h$ measures inactivation). Applying this model to cat motoneurones, the inactivation kinetics summarized in Figs. 8 and 9 can be combined with inward current measurements like those of Fig. 10 to yield the time course of the activation parameter M at a particular potential. The open circles in Fig. 10 plot the time course of M following a 30 mV depolarizing step. M values at early times are not well fitted by a single exponential, but are better fitted by the cubed exponential function drawn in Fig. 10, suggesting that the

depolarization-induced activation of inward current channels in cat motoneurones increases non-linearly with time, as in squid axons and other excitable membranes. Another observation suggesting non-linear activation is that two brief depolarizing pulses, each sufficient to activate only a small proportion of the inward current channels, yield a more than additive activation when they occur within 1 msec of each other. Our data were not sufficiently accurate to allow further characterization of this non-linear activation.

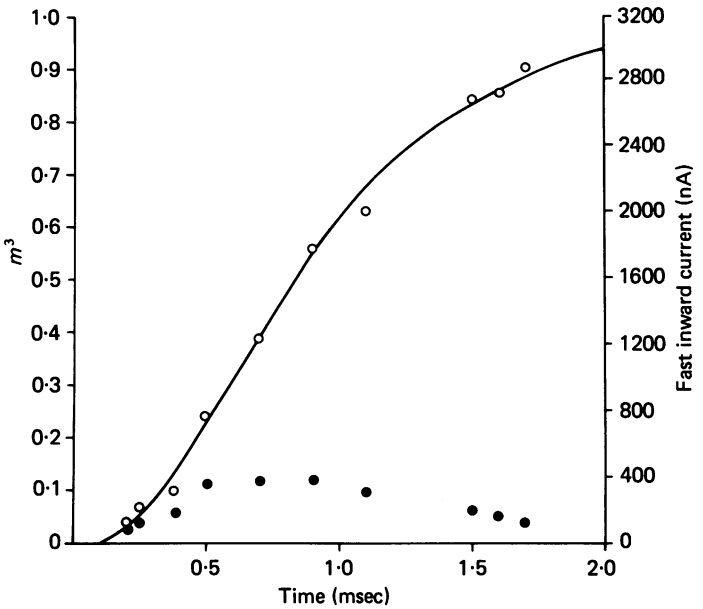

Fig. 10. Activation of the fast inward current as a function of time following a step depolarization from −10 mV to +30 mV. Filled circles plot inward current (right ordinate), extrapolated from inward current tails as described in the text. Open circles plot the activation parameter M (left ordinate), calculated by dividing the inward current by the predicted value of the h parameter at that voltage and time. The initial and steady-state values of h were assumed to be 1 and 0, respectively (Fig. 9); the time constant of decay of h at +30 mV is 0·58 msec (Fig. 8). In the Hodgkin–Huxley model M is proportional to the inward current expected in the absence of inactivation. The continuous line was drawn assuming that $M = m^3$, where $m = (1-\exp(-t/\tau_m))$ and $\tau_m = 0{\cdot}53$ msec, and was normalized to a steady-state value of 1.

DISCUSSION

The fast inward current of cat motoneurones is similar in many respects to the fast sodium current described in squid axon, frog node and many other excitable tissues (reviewed by Hille, 1970). The estimated reversal potential of +80 to +116 mV (relative to the resting potential, Fig. 5) and the inhibition produced by tetrodotoxin suggest that the major current carrier is sodium. Our values for the reversal potential of this fast inward current are close to the value of 120 mV estimated by Araki & Terzuolo (1962), and our maximal peak inward currents (400–450 nA) agree with those reported by these workers and by Nelson & Frank (1967). The peak amplitude

of this and other membrane currents undoubtedly varies with the size of the motoneurone. The relatively large amplitude of the inward current and the relatively low input resistance of the motoneurone of Figs. 3–9 and the motoneurones described in earlier voltage clamp studies suggest that these neurones were among the larger α-motoneurones.

This fast inward current is both activated and inactivated by depolarization. The development of inactivation at depolarized voltage levels and the recovery from inactivation at membrane potentials near the resting potential (Fig. 7) follow exponential time courses, whose time constants and steady-state values are functions only of membrane potential (Figs. 8, 9). The longest values of the inactivation time constant, τ_h, in these motoneurones, 1·0–1·3 msec, occur at potentials 10–20 mV negative to the resting potential, where the steady-state value of the inactivation parameter, h_∞, is near 1. This relationship between τ_h and h_∞ is different from that found in squid axon and frog node of Ranvier, where maximal τ_h values occur in the voltage range where h_∞ is about 0·5 (Figs. 3:32 and 4:58 in Cole, 1968). When this unusual relationship between τ_h and h_∞ in cat motoneurones is fitted with the formal Hodgkin–Huxley (1952*b*) equations, there is a greater than normal degree of overlap between the curves relating the voltage dependence of the forward and backward rate constants. The relatively long inactivation time constant near the resting potential in motoneurone somata would slow recovery from inactivation after an action potential, thus tending to suppress bursting behaviour.

It was more difficult to quantify the voltage-dependent activation of the inward current because of uncertainties in correcting for superimposed capacitative and initial segment currents, but indirect evidence (e.g. Fig. 10) suggests that activation begins with a slight delay and probably involves higher-order kinetics similar to those used to describe inward Na current activation in other excitable cells.

The extent to which the dendrites of normal (non-chromatolysed) cat motoneurones are invaded by action potentials remains unresolved. Our data do not rule out the possibility that dendrites have voltage-dependent conductance systems that contribute to action potentials invading the dendrites from the soma. However, arguments summarized in Results indicate that most of the inward currents in our selected motoneurones were under good voltage clamp control, and that contamination by voltage-sensitive currents from non-clamped dendritic membranes was negligible. This conclusion is supported by Fig. 13 of Barrett *et al.* (1980), which illustrates the good correspondence between the amplitude and rise time of the measured (non-clamped) action potential and a simulated action potential calculated using voltage clamp measurements of inward current magnitudes (Figs. 5, 10) and inactivation kinetics (Figs. 8, 9) and the non-linear Hodgkin–Huxley activation kinetics inferred from the analysis of Fig. 10.

Cat motoneurones (Liebl & Lux, 1975; Schwindt & Crill, 1977) as well as frog motoneurones (Barrett & Barrett, 1976) have a slow inward current distinct from the tetrodotoxin-sensitive fast inward Na current characterized here. We detected this slow inward current only in motoneurones injected electrophoretically with tetraethylammonium ions, which block both fast and slow outward currents when applied *intra*cellularly in motoneurones. These injected motoneurones showed, in addition to the fast inward current, an additional small (10–40 nA peak amplitude) inward

current that did not inactivate rapidly even at depolarizations exceeding +30 mV. In the absence of tetraethylammonium injections, this small, slow inward current is obscured by the much larger outward K currents.

We thank Drs E. Barrett and K. Magleby for reading the manuscript and A. Toro for preparing the manuscript. Supported by research grants NS-12207, VA-1610 and GM-00739.

REFERENCES

ARAKI, T. & TERZUOLO, C. A. (1962). Membrane currents in spinal motoneurons associated with the action potential and synaptic activity. *J. Neurophysiol.* **25**, 772–789.

BARRETT, E. F. & BARRETT, J. N. (1976). Separation of two voltage-sensitive potassium currents, and demonstration of a tetrodotoxin-resistant calcium current in frog motoneurones. *J. Physiol.* **255**, 737–774.

BARRETT, E. F., BARRETT, J. N. & CRILL, W. E. (1980). Voltage-sensitive outward currents in cat motoneurones. *J. Physiol.* **304**, 251–276.

BARRETT, J. N. & CRILL, W. E. (1974*a*). Specific membrane properties of cat motoneurones. *J. Physiol.* **239**, 301–324.

BARRETT, J. N. & CRILL, W. E. (1974*b*). Influence of dendritic location and membrane properties on the effectiveness of synapses on cat motoneurones. *J. Physiol.* **239**, 325–345.

BARRETT, J. N. & WHITLOCK, D. G. (1973). Technique for beveling glass microelectrodes. In *Intracellular Staining in Neurobiology*, ed. KATER, S. B. & NICHOLSON, C. New York: Springer-Verlag.

BEZANILLA, F. & ARMSTRONG, C. (1977). Inactivation of the sodium channel. 1. Sodium current experiments. *J. gen. Physiol.* **70**, 549–566.

BEZANILLA, F., ROJAS, E. & TAYLOR, R. E. (1970). Sodium and potassium conductance changes during a membrane action potential. *J. Physiol.* **211**, 729–751.

BLANKENSHIP, J. E. (1968). Action of tetrodotoxin on spinal motoneurons of the cat. *J. Neurophysiol.* **31**, 186–194.

BROWN, K. T. & FLAMING, D. G. (1975). Instrumentation and technique for beveling fine micropipette electrodes. *Brain Res.* **86**, 172–180.

BURKE, R. E. & TEN BRUGGENCATE, G. (1971). Electrotonic characteristics of alpha motoneurones of varying size. *J. Physiol.* **212**, 1–20.

CHIU, S. Y. (1977). Inactivation of sodium channels: second order kinetics in myelinated nerve. *J. Physiol.* **273**, 573–596.

COLE, K. S. (1968). *Membranes, Ions and Impulses*. Berkeley: University of California Press.

CONRADI, S. (1969). Observations on the ultrastructure of the axon hillock and initial axon segment of lumbosacral motoneurons in the cat. *Acta physiol. scand.* **78**, suppl. **332**, 65–85.

CONTI, F., HILLE, B., NEUMCKE, B., NONNER, W. & STAMPFLI, R. (1976). Measurement of the conductance of the sodium channel from current fluctuations at the node of Ranvier. *J. Physiol.* **262**, 699–727.

ECCLES, J. C., LIBET, B. & YOUNG, R. R. (1958). The behaviour of chromatolysed motoneurones studied by intracellular recording. *J. Physiol.* **143**, 11–40.

HILLE, B. (1970). Ionic channels in nerve membranes. *Prog. Biophys. Biol.* **21**, 3–32.

HILLE, B. (1976). Gating in sodium channels of nerve. *A. Rev. Physiol.* **38**, 139–152.

HODGKIN, A. L. & HUXLEY, A. F. (1952*a*). The dual effect of membrane potential on sodium conductance in the giant axon of *Loligo*. *J. Physiol.* **116**, 497–506.

HODGKIN, A. L. & HUXLEY, A. F. (1952*b*). A quantitative description of membrane current and its application to conduction and excitation in nerve. *J. Physiol.* **117**, 500–544.

JACK, J. J. B. & REDMAN, S. J. (1971). An electrical description of the motoneurone, and its application to the analysis of synaptic potentials. *J. Physiol.* **215**, 321–352.

KRIPKE, B. R. & OGDEN, T. E. (1974). A technique for beveling fine micropipettes. *Electroenceph. clin. Neurophysiol.* **36**, 323–326.

KUNO, M. & LLINÁS, R. (1970). Enhancement of synaptic transmission by dendritic potentials in chromatolysed motoneurones of the cat. *J. Physiol.* **210**, 807–821.

LIEBL, L. & LUX, H. D. (1975). The action of Co^{++}, Ba^{++} and verapamil in anomalous rectification in cat spinal motoneurons. *Pflugers Arch.* **355**, R80.

LUX, H. D., SCHUBERT, P. & KREUTZBERG, G. W. (1970). Direct matching of morphological and electrophysiological data in cat spinal motorneurons. In *Excitatory Synaptic Mechanisms*, ed. ANDERSEN, P. & JANSEN, J., pp. 189–198. Oslo: Universitetsforlaget.

NELSON, P. G. & FRANK, K. (1964). La production du potentiel d'action étudiée par la technique du voltage imposée sur le motoneurone du chat. *Actual. neurophysiol.* **5**, 15–35.

NELSON, P. G. & LUX, H. D. (1970). Some electrical measurements of motoneuron parameters. *Biophys. J.* **10**, 55–73.

OGDEN, T. E., CITRON, M. C. & PIERANTONI, R. (1978). The jet stream microbeveler: an inexpensive way to bevel ultrafine glass micropipettes. *Science, N.Y.* **201**, 469–470.

PEACOCK, J., NELSON, P. G. & GOLDSTONE, M. W. (1973). Electrophysiologic study of cultured neurons dissociated from spinal cords and dorsal root ganglia of fetal mice. *Devl Biol.* **30**, 137–152.

RALL, W. (1969). Time constants and electrotonic length of membrane cylinders and neurons. *Biophys. J.* **9**, 1483–1508.

SCHWINDT, P. & CRILL, W. E. (1977). A persistent negative resistance in cat lumbar motoneurones. *Brain Res.* **120**, 173–178.